

# Ultradilute self-bound quantum droplets in Bose-Bose mixtures at finite temperature

Jia Wang, Xia-Ji Liu, and Hui Hu

Centre for Quantum Technology Theory, Swinburne University of Technology, Melbourne, Victoria 3122, Australia

(Dated: October 29, 2020)

We theoretically investigate the finite-temperature structure and collective excitations of a self-bound ultradilute Bose droplet in a flat space realized in a binary Bose mixture with attractive inter-species interactions on the verge of mean-field collapse. As the droplet formation relies critically on the repulsive force provided by Lee-Huang-Yang quantum fluctuations, which can be easily compensated by thermal fluctuations, we find a significant temperature effect in the density distribution and collective excitation spectrum of the Bose droplet. A finite-temperature phase diagram as a function of the number of particles is determined. We show that the critical number of particles at the droplet-to-gas transition increases dramatically with increasing temperature. Towards the bulk threshold temperature for thermally destabilizing an infinitely large droplet, we find that the excitation-forbidden, self-evaporation region in the excitation spectrum, predicted earlier by Petrov using a zero-temperature theory, shrinks and eventually disappears. All the collective excitations, including both surface modes and compressional bulk modes, become softened at the droplet-to-gas transition. The predicted temperature effects of a self-bound Bose droplet in this work could be difficult to measure experimentally due to the lack of efficient thermometry at low temperatures. However, these effects may already present in the current cold-atom experiments.

## I. INTRODUCTION

The recent observation of an ultradilute self-bound droplet-like state [1] in single-component dipolar Bose-Einstein condensates (BECs) [2–5] and binary Bose-Bose mixtures [6–11] opens an entirely new direction to better understand the fascinating concept of quantum droplets - autonomously isolated quantum systems equilibrated under *zero* pressure in free space. Quantum droplets such as helium nano-droplets have already been intensively investigated in condensed matter community over the past few decades [12, 13]. However, an in-depth understanding of helium nano-droplets is still lacking, due to the strong inter-particle interactions and the limited techniques to control and characterize the nano-droplets. These limitations could be overcome for ultradilute Bose droplets, owing to the unprecedented controllability in cold-atom experiments [14]. For example, the inter-particle interactions in Bose droplets can be tuned at will by using Feshbach resonances [15] and their structure and collective excitations can be accurately measured through in-situ or time-of-flight absorption imaging [14]. In particular, the realization of a weakly interacting Bose droplet now allows us to develop quantitative descriptions and make it possible to have testable theoretical predictions [16–35].

In this respect, it is worth noting the seminal work by Petrov [16], where the existence of a Bose droplet is proposed in binary Bose mixtures with attractive inter-species attractions. The mean-field collapse is surprisingly shown to be arrested by an effective repulsive force arising from Lee-Huang-Yang (LHY) quantum fluctuations [36]. This ground-breaking proposal is now successfully confirmed in several experimental setups, including the homonuclear  $^{39}\text{K}$ - $^{39}\text{K}$  mixtures [6–9] and heteronuclear  $^{41}\text{K}$ - $^{87}\text{Rb}$  [10] or  $^{23}\text{Na}$ - $^{87}\text{Rb}$  mixtures [11]. Following Petrov's pioneering idea [16], numerous theoretical investigations have been recently carried out [16–26, 28–

35], addressing various zero-temperature properties of Bose droplets.

The finite-temperature properties of Bose droplets in both dipolar BECs and binary Bose mixtures, however, do not receive too much attention. Ultradilute droplets of dipolar bosons at finite temperature have recently been considered in the presence of an external harmonic trap [27]. For Bose droplets in binary mixtures, only the *bulk* properties (of an infinitely large droplet) at nonzero temperature are addressed most recently [37, 38]. As the effective repulsive force provided by the LHY fluctuation term can be easily neutralized by thermal fluctuations, it is not a surprise to find that a Bose droplet in binary mixtures can be completely destabilized above a threshold temperature  $T_{\text{th}}$  [37].

The less interest in the finite temperature effect is probably due to the peculiar *self-evaporation* feature of quantum droplets. As a self-bound entity, the energy of elementary excitations of quantum droplets - either single-particle excitations or collective excitations - has to be bounded from above by the so-called particle-emission threshold, making the droplet essentially a low-temperature object. This is fairly evident in helium nano-droplets: once the nano-droplet is created, its temperature rapidly decreases to about 0.4 Kelvin in several milliseconds [12]. Afterward, however, the self-evaporation becomes not so efficient [12]. A Bose droplet in a binary mixture is similarly anticipated to be a low-temperature object. In particular, as predicted by Petrov from zero-temperature calculations [16], for the number of particles in a certain range, there are no collective excitations below the particle-emission threshold. In other words, an excitation-forbidden region in the particle number exists. The Bose droplet then may automatically lose its thermal energy upon releasing the most energetic particles and reach exactly zero temperature.

In this work, we would like to argue that the self-

evaporation efficiency of Bose droplets at low temperature could be much reduced, as in helium nano-droplets [12]. As a result, the experimentally observed Bose droplets might have a small but nonzero temperature in the realistic time-scale of experiments [6–9]. We theoretically determine the finite-temperature structure and collective excitations of self-bound spherical Bose droplets with a finite number of particles, based on time-independent and time-dependent extended Gross-Pitaevskii equations (GPEs) [16], respectively. We find a rich phase diagram at finite temperature. In particular, the excitation-forbidden, self-evaporation region of the Bose droplet, found earlier by Petrov using a zero-temperature theory [16], turns out to shrink with increasing temperature and disappears eventually. We also predict that the surface modes and compressional sound modes of the Bose droplet become softened at the droplet-to-gas transition upon increasing temperature. Our results could be experimentally examined in binary Bose mixtures if efficient thermometry can be established at low temperatures.

## II. EXTENDED GROSS-PITAEVSKII EQUATION AT FINITE TEMPERATURE

To address the finite-temperature properties of a finite-size Bose droplet, we consider the *finite-temperature* version of the extended GPE,

$$i\hbar \frac{\partial \Phi}{\partial t} = \left[ -\frac{\hbar^2}{2m} \nabla^2 - \mu + \frac{\partial \mathcal{F}}{\partial n} \left( n = |\Phi|^2 \right) \right] \Phi, \quad (1)$$

where  $\Phi(\mathbf{x}, t)$  can be treated as the wave-function of the Bose droplet with atomic mass  $m$ ,  $\mu$  is the chemical potential to be determined by the total number of particles  $N$ , and  $\mathcal{F}(n)$  is the local *free* energy functional (per unit volume  $\mathcal{V}$ ) depending on the local density  $n(\mathbf{x}, t) = |\Phi(\mathbf{x}, t)|^2$ . At zero temperature, the free energy functional  $\mathcal{F}(n)$  reduces to the ground-state energy functional  $\mathcal{E}(n)$  [16], and we recover the zero-temperature extended GPE [16] that has been extensively used in the literature.

In a binary Bose mixture, the extended GPE Eq. (1) for Bose droplets can be microscopically derived by using a bosonic pairing theory [32, 33]. This was demonstrated in the recent work at zero temperature under the local density approximation [34]. The generalization of such a derivation to the nonzero temperature  $T \neq 0$  is straightforward. It is easy to show that the free energy functional per unit volume could take the form [37],

$$\mathcal{F} = -\frac{\pi\hbar^2}{m} \left( a + \frac{a^2}{a_{12}} \right) n^2 + \frac{256\sqrt{\pi}}{15} \left( \frac{\hbar^2 a^{5/2}}{m} \right) n^{5/2} - \frac{\sqrt{\pi}}{720} \left( \frac{m^3 k_B^4 T^4}{\hbar^6 a^{3/2}} \right) n^{-3/2} \tilde{s}_3(1, \gamma), \quad (2)$$

where  $a > 0$  and  $a_{12} \simeq -a$  are the intra-species and inter-species  $s$ -wave scattering lengths of the binary Bose mixture, respectively. The last term in the above expression

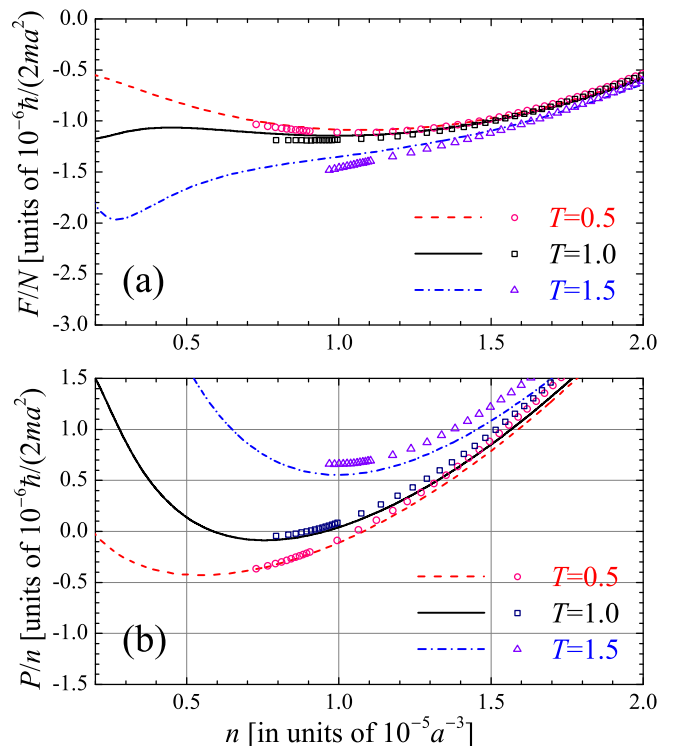


FIG. 1. Equation of state (EoS). The free energy per particle  $\mathcal{F}/n$  (a) and pressure per particle  $P/n$  (b) of a homogeneous binary Bose mixture, in units of  $10^{-6}\hbar^2/(2ma^2)$ , are shown as a function of the density  $n$  at three temperatures  $k_B T = 0.5, 1.0$  and  $1.5$ . The density  $n$  and temperature  $T$  are measured in units of  $10^{-5}a^{-3}$  and  $10^{-4}\hbar^2/(2ma^2)$ , respectively. A self-bound Bose droplet is realized, when the pressure is zero at an equilibrium density  $n_0$ . The symbols and lines show the numerical and analytical results, respectively. The former is from a bosonic pairing theory, while the latter is calculated according to Eq. (2) and Eq. (3). We note that the numerical results are not available at sufficiently low density. Here, we consider the inter-species interaction strength  $a_{12} = -1.05a$ .

accounts for the finite-temperature effect and the function  $\tilde{s}_3[1, \gamma \equiv mk_B T / (2\pi\hbar^2 an)]$  could be calculated numerically [37]. It becomes unity in the zero-temperature limit and decreases with increasing temperature [37]. It turns out that close to the threshold for the formation of Bose droplets, i.e.,  $a_{12} \simeq -a$ , the function  $\tilde{s}_3(1, \gamma)$  could be reasonably approximated by an exponential decay form at low temperature, i.e.,

$$s_3(1, \gamma) \simeq \exp(-A\gamma), \quad (3)$$

with a decay constant  $A \simeq 0.5$ . This is shown in Fig. 1(a), where the predictions of Eq. (2) and Eq. (3) are compared with the numerical results from the bosonic pairing theory [37]. Eq. (2) also enables us to calculate the pressure by using the standard thermodynamic relation,  $P = n^2[\partial(\mathcal{F}/n)/\partial n]$ . It is evident from Fig. 1(b) that the zero-pressure condition, which is required for a self-bound Bose droplet, can not be satisfied for relatively large temperature (i.e.,  $T = 1.5 \times 10^{-4}\hbar^2/(2ma^2)$ ). In-

deed, from the analysis of our previous work [37], we find that an infinitely large Bose droplet thermally dissolves itself once the temperature is above a threshold,

$$k_B T_{\text{th}} \simeq 0.0222 \left(1 + \frac{a}{a_{12}}\right)^2 \frac{\hbar^2}{ma^2}. \quad (4)$$

For the inter-species interaction strength considered in Fig. 1,  $a_{12} = -1.05a$ , the threshold temperature is about  $k_B T_{\text{th}} \simeq 5.03 \times 10^{-5} \hbar^2 / (ma^2)$ . To be specific, we will concentrate on this example with  $a_{12} = -1.05a$ . But, it will become clear later that our results do not depend on this particular choice of the interaction parameters.

It is useful to note that an exponential decay form of the function  $\tilde{s}_3(1, \gamma)$  is very helpful for our numerical solutions of the extended GPE. This exponential decay, i.e.,  $e^{-B/n}$  with  $B \equiv Amk_B T / (2\pi\hbar^2 a)$ , largely compensates the power-law increase  $n^{-3/2}$  in the last term of the free energy Eq. (2) at low density and therefore remove the possible numerical instability caused by the sufficiently low density at the edge of the Bose droplet.

To ease the numerical workload, it is also helpful to use the (dimensionless) re-scaled coordinate and time as suggested by Petrov in his pioneering work [16]:

$$\tilde{\mathbf{x}} = \frac{\mathbf{x}}{\xi}, \quad (5)$$

$$\tilde{t} = \frac{t}{m\xi^2/\hbar}, \quad (6)$$

$$\phi = \frac{\Phi}{\sqrt{n_0}}, \quad (7)$$

$$\tilde{\mu} = \frac{\mu}{\hbar^2 / (m\xi^2)}, \quad (8)$$

where the equilibrium (bulk) density  $n_0$  of a large Bose droplet at zero temperature is [32]

$$n_0 \equiv \frac{25\pi}{16384} \left(1 + \frac{a}{a_{12}}\right)^2 a^{-3} \quad (9)$$

and the length scale  $\xi$  can be chosen in such a way that the ground-state energy functional (i.e., the free energy functional at zero temperature) per unit volume takes the form  $\mathcal{E} = -3|\phi|^4/2 + |\phi|^5$  [16]. This leads to the energy scale,

$$\frac{\hbar^2}{m\xi^2} = \frac{25\pi^2}{24576} \left(1 + \frac{a}{a_{12}}\right)^3 \frac{\hbar^2}{ma^2}. \quad (10)$$

At  $a_{12} = -1.05a$ , we find the energy units  $\hbar^2 / (m\xi^2) \simeq 1.08 \times 10^{-6} \hbar^2 / (ma^2)$  and the units for the number of particles  $n_0 \xi^3 = N/\tilde{N} \simeq 9630$ , where  $\tilde{N}$  is the reduced number of particles. In terms of the energy scale  $\hbar^2 / (m\xi^2)$ , we may re-write the threshold temperature,

$$k_B T_{\text{th}} \simeq 2.21 \left(1 + \frac{a}{a_{12}}\right)^{-1} \frac{\hbar^2}{m\xi^2}, \quad (11)$$

which is about  $46.4\hbar^2 / (m\xi^2)$  at  $a_{12} = -1.05a$ .

From now on, without any confusion we shall remove the tilde above the re-scaled quantities. The time-dependent extended GPE then takes the following *dimensionless* form,

$$i \frac{\partial}{\partial t} \phi = \left[ -\frac{1}{2} \nabla^2 - \mu + \frac{\partial \mathcal{F}}{\partial n}(\phi, \phi^*) \right] \phi, \quad (12)$$

where the dimensionless free energy functional is now given by (the density  $n = |\phi|^2$ ),

$$\mathcal{F} = -\frac{3}{2} |\phi|^4 + |\phi|^5 - \frac{C_T}{|\phi|^3} \exp \left[ -\frac{B_T}{|\phi|^2} \right] \quad (13)$$

with the temperature-dependent constants,

$$C_T \equiv \frac{\pi^4}{62208} \left[ \frac{(1 + a/a_{12}) k_B T}{\hbar^2 / (m\xi^2)} \right]^4 \simeq 0.0374 \frac{T^4}{T_{\text{th}}^4}, \quad (14)$$

$$B_T \equiv \frac{A}{3} \left(1 + \frac{a}{a_{12}}\right) \frac{k_B T}{\hbar^2 / (m\xi^2)} \simeq 0.369 \frac{T}{T_{\text{th}}}. \quad (15)$$

At zero temperature, where the last term in Eq. (13) is absent, Eq. (12) recovers the dimensionless extended GPE used earlier by Petrov [16]. The two temperature-dependent constants  $C_T$  and  $B_T$  are the function of the ratio  $T/T_{\text{th}}$  only and do not depend explicitly on the scattering lengths  $a$  and  $a_{12}$ . Near the threshold temperature  $T \sim T_{\text{th}}$ , both constants become significant, and we find that the LHY quantum-fluctuation term ( $\propto |\phi|^5$ ) in the free energy functional is largely compensated by the last thermal-fluctuation term. This eventually destabilizes a large Bose droplet at the threshold temperature  $T_{\text{th}}$  [37]. Let us now analyze how does this thermal destabilization occur for a Bose droplet with a finite (reduced) number of particles.

### A. Time-independent GPE for the density distribution $\phi_0$

In free space, the self-bound Bose droplet takes an isotropic spherical profile, depending on the radius  $r$  only [8, 16]. The static profile  $\phi_0(r) \geq 0$  at finite temperature satisfies the time-independent version of Eq. (12):

$$\hat{\mathcal{L}}\phi_0(r) = \mu\phi_0(r), \quad (16)$$

where we have defined the operator,

$$\hat{\mathcal{L}} \equiv -\frac{\nabla^2}{2} - 3\phi_0^2 + \frac{5}{2}\phi_0^3 + \frac{\partial \mathcal{F}_T}{\partial n}. \quad (17)$$

The last term of the thermal contribution to  $\hat{\mathcal{L}}$  is explicitly given by,

$$\frac{\partial \mathcal{F}_T}{\partial n} = +\frac{3C_T}{2\phi_0^5} \left(1 - \frac{2B_T}{3\phi_0^2}\right) \exp \left[ -\frac{B_T}{\phi_0^2} \right]. \quad (18)$$

In this work, we solve the static GPE numerically via a gradient method, which improves the accuracy and efficiency from our previous work [14, 39, 40]. The details of our numerical method are described in the Appendix.

## B. Bogoliubov equations for collective excitations

To study the collective excitations of the Bose droplet, we consider small fluctuation modes around the condensate wave-function  $\phi_0(r)$  [14, 31, 40],

$$\phi(\mathbf{x}, t) = \phi_0(r) + \sum_j [u_j(\mathbf{x}) e^{-i\omega_j t} + v_j^*(\mathbf{x}) e^{+i\omega_j t}], \quad (19)$$

where different mode with mode frequency  $\omega_j$  is indexed by an integer  $j$ , and  $u_j(\mathbf{x})$  and  $v_j(\mathbf{x})$  are the corresponding mode wave-functions. For a spherical droplet, the index  $j$  can be further denoted by two good quantum numbers  $(l, n)$ , where  $l$  is the angular momentum and  $n$  stands for the radial quantum number (i.e., the number of nodes in the radial wave-function). By substituting the above expression into the dimensionless extended GPE Eq. (12) and expanding it to the linear order in  $u_j(\mathbf{x})$  and  $v_j(\mathbf{x})$ , we obtain the celebrated Bogoliubov equations [14, 31, 40],

$$\begin{bmatrix} \hat{\mathcal{L}} - \mu + \hat{\mathcal{M}} & \hat{\mathcal{M}} \\ \hat{\mathcal{M}} & \hat{\mathcal{L}} - \mu + \hat{\mathcal{M}} \end{bmatrix} \begin{bmatrix} u_j(\mathbf{r}) \\ v_j(\mathbf{r}) \end{bmatrix} = \omega_j \begin{bmatrix} +u_j(\mathbf{r}) \\ -v_j(\mathbf{r}) \end{bmatrix}, \quad (20)$$

where the operator  $\hat{\mathcal{M}}$  is given by,

$$\hat{\mathcal{M}} \equiv n \frac{\partial^2 \mathcal{F}}{\partial n^2} = -3\phi_0^2 + \frac{15}{4}\phi_0^3 + n \frac{\partial^2 \mathcal{F}_T}{\partial n^2}, \quad (21)$$

and the explicit form of the last thermal term in  $\hat{\mathcal{M}}$  is,

$$n \frac{\partial^2 \mathcal{F}_T}{\partial n^2} = -\frac{15C_T}{4\phi_0^5} \left( 1 - \frac{4B_T}{3\phi_0^2} + \frac{4B_T^2}{15\phi_0^4} \right) \exp \left[ -\frac{B_T}{\phi_0^2} \right]. \quad (22)$$

It should be noted that the wave-functions  $u(\mathbf{x}) = +\phi_0(r)$  and  $v(\mathbf{x}) = -\phi_0(r)$  are the zero-energy solution (i.e.,  $\omega_j = 0$ ) of the Bogoliubov equations. This is precisely the condensate mode of the Bose droplet and therefore should be discarded. To numerically solve the Bogoliubov equations, we follow the technique by Hutchinson, Zaremba and Griffin [41]. The details of the numerical implementation can be found in Ref. [40] and the Appendix.

## III. RESULTS AND DISCUSSIONS

For a given reduced number of particles  $N$  and a given reduced temperature (i.e., the ratio  $T/T_{\text{th}}$ ), we have numerically solved the dimensionless static GPE Eq. (16) and Bogoliubov equations Eq. (20) for the density distribution  $\phi_0(r)$  and the collective excitation spectrum  $\omega_j$ , respectively. To connect with the experimental observables at different scattering lengths  $a$  and  $a_{12}$ , we can restore the units of different quantities (i.e., density, mode frequency and temperature) by simply multiplying, for example, the equilibrium density  $n_0$ , the energy scale  $\hbar^2/(m\xi^2)$  and the temperature scale  $T_{\text{th}}$ , which are given in Eq. (9), Eq. (10) and Eq. (11), respectively.

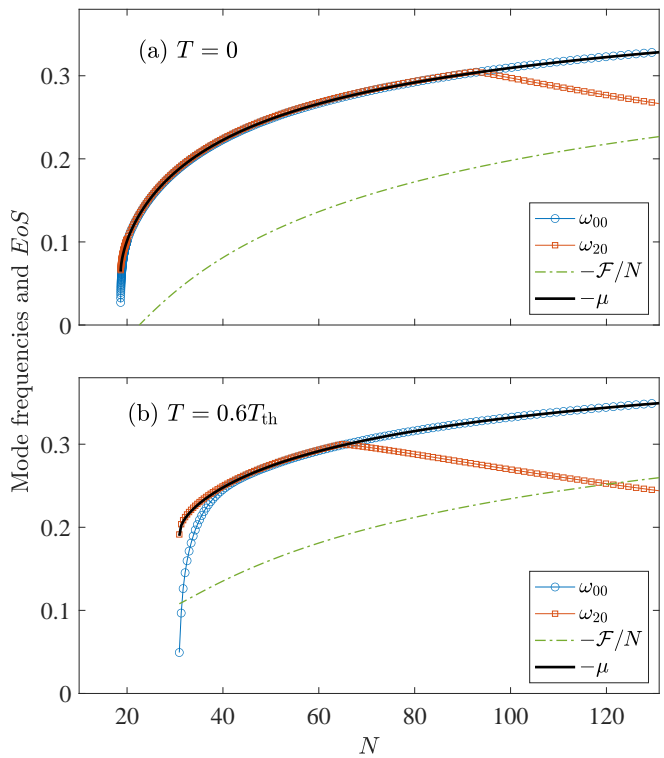


FIG. 2. The chemical potential  $-\mu$  (black solid curves), free energy per particle  $-\mathcal{F}/N$  (green dash-dotted curves), breathing mode frequency (blue open circles with curves), and the quadrupole mode frequency (red open squares with curves) as a function of the number of particle at zero temperature (a) and at temperature  $T = 0.6T_{\text{th}}$  (b). At zero temperature in (a), a metastable Bose droplet occurs when the number of particles decreases down to  $N_m \simeq 22.55$ , when the free energy  $\mathcal{F}$  becomes positive (or  $-\mathcal{F}$  becomes negative).

In the following, we first consider the excitation spectrum at some chosen temperatures and determine a rich finite-temperature phase diagram. We then discuss in detail the temperature dependence of the density distribution and excitation spectrum at fixed number of particles, mimicking the realistic experimental measurements with running temperature.

### A. Collective excitations at a given temperature

To start, let us briefly review the essential zero-temperature properties of a self-bound Bose droplet [16]. First, the chemical potential  $\mu$  of the droplet has to be negative ( $\mu < 0$ ), less than that of the surrounding vacuum (i.e.,  $\mu_{\text{vac}} = 0$ ). Otherwise, it is not energetically favorable for particles to be added into the droplet. For an infinitely large droplet, where the edge effect can be safely neglected, it is clear from the stationary GPE Eq. (16) that the condensate wave-function in the bulk is  $\phi_0 = 1$  in the re-scale units and the chemical potential  $\mu = -1/2$ . As we decrease the number of particles in the droplet,

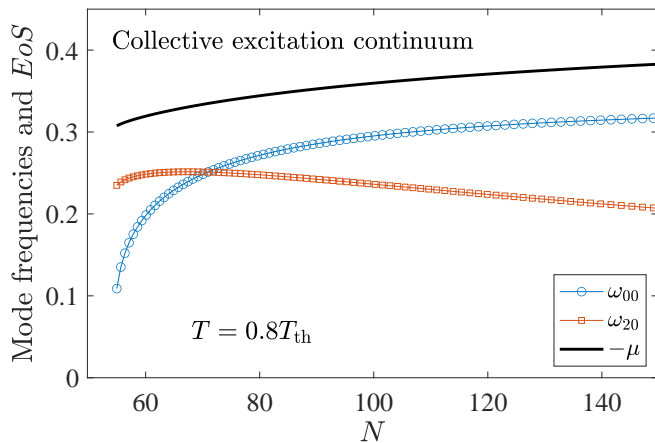


FIG. 3. The chemical potential  $-\mu$  (black lines), breathing mode frequency (blue solid circles with lines), and the quadrupole mode frequency (red open squares with lines) as a function of the number of particle at temperature  $T = 0.8T_{\text{th}}$  (b).

the wave-function  $\phi_0(r)$  will be smaller than unity and the chemical potential increases towards  $\mu \rightarrow 0^-$ . The droplet will eventually become unstable and experience a droplet-to-gas transition, when the zero-pressure condition for the droplet state is strongly violated at low density. The droplet-to-gas transition at the critical number of particles  $N_c \simeq 18.65$  has been analyzed in detail by Petrov [16], by considering the balance between the kinetic energy (i.e. from the Laplace operator  $-\nabla^2/2$ ) and the interaction energy (i.e.,  $\mathcal{F}(\phi_0)$ ). The transition is clearly signaled by the softening of the breathing mode frequency  $\omega_{l=0,n=0}$ , which vanishes precisely at  $N_c$ . This is shown by blue circles in Fig. 2(a), where we reproduce the lower panel of Fig. 1 in Ref. [16]. Petrov also predicted the existence of a metastable droplet state when the number of particles is slightly larger than the critical number, i.e.,  $N_c < N < N_m \simeq 22.55$  [16]. This metastable state has a positive total energy, i.e.,  $-\mathcal{F} < 0$  as shown in Fig. 2(a), so the particles in the droplet will eventually escape to the vacuum via tunneling through an energy barrier (created by the competing kinetic and interaction energies).

Another interesting zero-temperature feature of the Bose droplet is the existence of an excitation-forbidden window in the number of particles [16], as we mentioned earlier. In Fig. 2(a), there is no collective excitations in the stable droplet state below a threshold number of particles,  $N < N_{\text{th}} \simeq 94.2$ . All collective excitations are accumulated right above the particle-emission threshold  $|\mu|$ , forming an *unbounded* collective excitation continuum [40]. The bounded collective excitations are only possible at  $N > N_{\text{th}}$ , where the quadrupole mode frequency  $\omega_{l=2,n=0}$  first becomes smaller than  $|\mu|$  [16], as shown by the red empty squares. At sufficiently large number of particles (i.e.,  $N \sim 10^4$ ), the Bose droplet is able to acquire a series of the surface modes and compress-

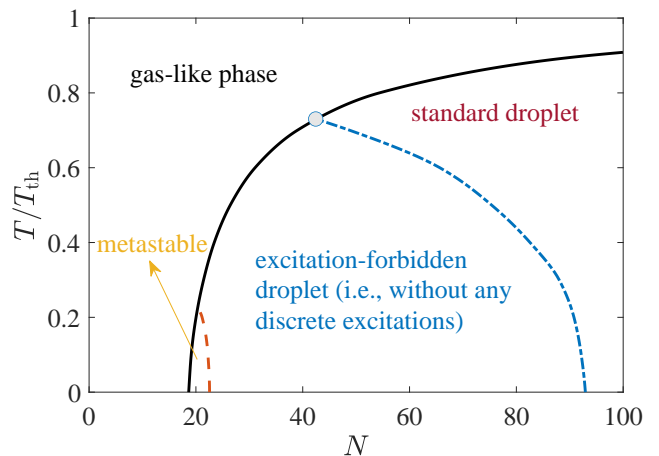


FIG. 4. The phase diagram of a finite-size Bose droplet as functions of the reduced number of particles  $N$  (horizontal axis) and of the reduced temperature  $T/T_{\text{th}}$  (vertical axis). At large temperature and small number of particles, the system is in the gas-like phase, while at low temperature and large number of particles, it is in the droplet state. A metastable droplet state also occurs at low temperature and relatively small number of particle.

sional sound modes with well-defined dispersion relations [16, 40], as we shall see later.

At finite temperature, the collective excitation spectrum can dramatically change. In Fig. 2(b), we report the excitation spectrum at  $T = 0.6T_{\text{th}}$ . It is readily seen that the droplet-to-gas transition now occurs at a much larger critical number of particles,  $N_c(T = 0.6T_{\text{th}}) \simeq 30.9$ , where the breathing mode frequency drops to zero. At the same time, the free energy  $\mathcal{F}$  is always negative, indicating that the metastable droplet state found at zero temperature does not exist anymore. The threshold number of particle for the excitation-forbidden window also significantly decreases and we find that  $N_{\text{th}}(T = 0.6T_{\text{th}}) \simeq 66.2$ . For  $N > 66.2$ , the quadrupole mode frequency  $\omega_{20}$  decreases with increasing number of particles, while the breathing mode frequency  $\omega_{00}$  continuously follows the particle-emission threshold  $|\mu|$  at the number of particles considered in the figure.

In Fig. 3, we show the excitation spectrum at an even larger temperature  $T = 0.8T_{\text{th}}$ . At this temperature, the excitation-forbidden window in the number of particles completely disappears. Both the breathing mode frequency and quadrupole mode frequency appear to be bounded below the particle-emission threshold  $|\mu|$ .

## B. A finite-temperature phase diagram

We have calculated the excitation spectrum at different reduced temperatures and consequently have obtained a finite-temperature phase diagram, as reported in Fig. 4. This presents the main result of our work. Here, the

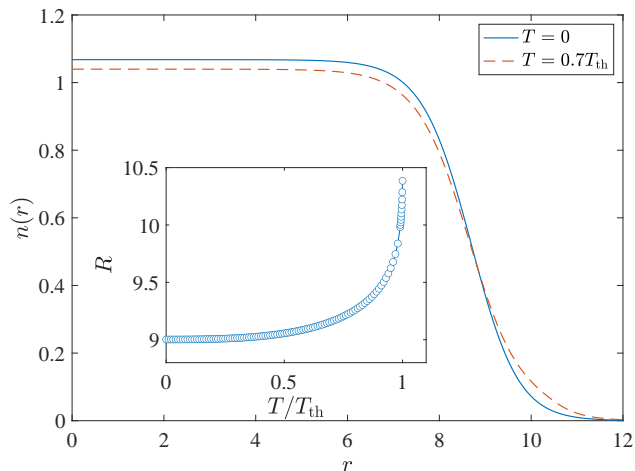


FIG. 5. The density distribution  $n(r)$  of a large self-bound Bose droplet ( $N = 3000$ ) at zero temperature (blue solid curve) and at the temperature  $T = 0.7T_{\text{th}}$  (red dashed curve). The inset shows the temperature dependence of the size of the Bose droplet, defined by  $R = \sqrt{5 \langle r^2 \rangle / 3}$ .

critical number of particle  $N_c$  (black solid curve) is determined by extrapolating the breathing mode frequency  $\omega_{00}$  to zero, and the critical number  $N_m$  (red dashed curve) is obtained by tracing the position where the free energy becomes positive. The two curves cross with each other at about  $0.24T_{\text{th}}$ , above which the window for a metastable droplet state closes. It is interesting to note that the critical number of particles  $N_c$  shows a sensitive temperature dependence. It increases very rapidly once the temperature is above about  $0.4T_{\text{th}}$ . Approaching the bulk threshold temperature  $T_{\text{th}}$ , a Bose droplet with any number of particles becomes thermally unstable, as we already show in the previous work [37].

On the other hand, the threshold number of particle  $N_{\text{th}}$  (blue dash-dotted curve) can be determined from the crossing point between the quadruple mode frequency  $\omega_{20}$  and the particle-emission threshold  $|\mu|$ . It separates the phase space for a stable Bose droplet into two regimes: an *excitation-forbidden* droplet regime without any bounded collective excitations below the particle-emission threshold and a *standard* droplet regime with at least one discrete collective excitation. With increasing temperature, we find that the  $N_{\text{th}}$ -curve terminates at about  $0.73T_{\text{th}}$  (see, i.e., the solid circle symbol in the figure). Above this temperature, we always find standard Bose droplets, in which a small but nonzero temperature or entropy could be accommodated by the discrete bounded collective excitations. Therefore, the intriguing self-evaporation phenomenon predicted by Petrov, i.e., the emission of particles upon arbitrary excitations [16], ceases to exist. The Bose droplets then fail to automatically reach zero temperature.

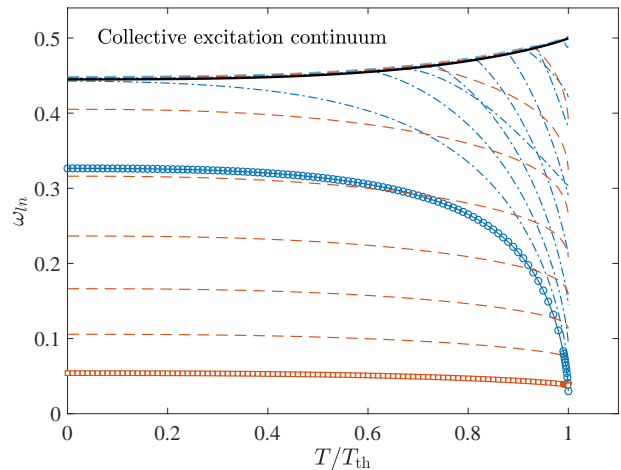


FIG. 6. Excitation frequencies  $\omega_{ln}$  ( $l \leq 9$  and  $n \leq 2$ ) of a large self-bound Bose droplet ( $N = 3000$ ), as a function of the reduced temperature  $T/T_{\text{th}}$ . The red dashed curves show the surface modes  $\omega_{l \geq 2, n=0}$  and the blue dash-dotted curves show the compressional bulk modes. The lowest surface mode  $\omega_{20}$  (i.e., quadruple mode) and the lowest bulk mode (breathing mode) are highlighted by the red open squares and blue open circles, respectively. The black thick curve shows the threshold  $-\mu$ .

### C. The temperature-dependences of the density distribution and collective excitations

Let us now consider an *idealized* experimental situation. Initially, a Bose droplet is nearly in thermal equilibrium at a nonzero temperature. It then gradually reduces its temperature by emitting a very small portion of the most energetic particles. This slow self-evaporation might be treated as an adiabatic process. By taking the in-situ or time-of-flight absorption imaging of the Bose droplet, we may then experimentally extract the temperature-dependences of the density distribution and collective excitations of the Bose droplet, at a nearly constant number of particles.

#### 1. Large Bose droplets

In Fig. 5, we present the density distribution of a large Bose droplet with the number of particles  $N = 3000$  at zero temperature (solid curve) and at  $T = 0.7T_{\text{th}}$  (dashed curve). For such a large droplet, the distribution acquires the typical flat-top structure [16]. Moreover, the temperature dependence of the density profile is not so apparent: the difference between the distributions at the two temperatures is less than 3%. This is correlated with a weak-temperature dependence of the droplet radius  $R$ , as shown in the inset, where the radius is defined as the square root of the mean square of the distance,  $R = \sqrt{5 \langle r^2 \rangle / 3}$ . The droplet size only increases notably when the temperature is close to the bulk thermal desta-

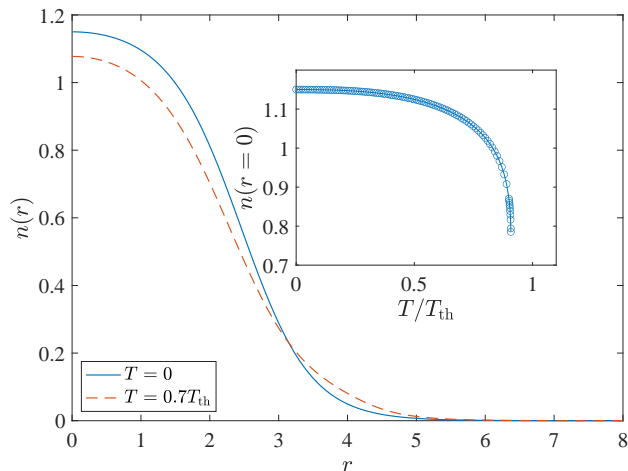


FIG. 7. The density distribution  $n(r)$  of a small self-bound Bose droplet ( $N = 100$ ) at zero temperature (blue solid curve) and at the temperature  $T = 0.7T_{\text{th}}$  (red dashed curve). The inset shows the temperature dependence of the center density at  $r = 0$ .

bilization threshold  $T_{\text{th}}$  (i.e.,  $T > T_{\text{th}}$ ).

In Fig. 6, we report the corresponding collective excitation spectrum as a function of the temperature. At zero temperature, there are a number of discrete modes, which can be well categorized as the surface modes ( $\omega_{l \geq 2, n=0}$ , red open squares and red dashed curves) and bulk modes ( $\omega_{00}$ , the breathing mode in blue circles; and  $\omega_{l, n \neq 0}$ , blue dash-dotted curves) [40]. The surface modes only propagate near the edge of the Bose droplet and have an exotic dispersion relation,  $\omega_{l0}^{(\text{surface})} \propto \sqrt{\sigma_s l(l-1)(l+2)}/R^{3/2}$ , with  $\sigma_s$  being the surface tension [12, 16]. In contrast, the bulk modes are compressional sound modes that propagate through the whole droplet and have the standard dispersion relation,  $\omega_{ln}^{(\text{bulk})} \propto c/R$ , where  $c$  is the bulk sound velocity [12, 40]. It is readily seen that the frequency of the low-lying surface modes does not change too much with increasing temperature. This could be understood from the robust flat-top and temperature insensitive density distribution as we observe in Fig. 5. As a result, the droplet size  $R$ , the surface tension  $\sigma_s$  and hence the surface mode frequencies are less dependent on the temperature. On the other hand, the frequency of the bulk sound modes has a strong temperature dependence and clearly shows a waterfall-like effect close to the bulk threshold temperature  $T_{\text{th}}$ . This is related to the softening of the sound velocity, which becomes exactly zero at the droplet-to-gas transition. All the bulk mode frequencies therefore have to vanish towards the transition.

## 2. Small Bose droplets

Let us now consider a Bose droplet with small reduced number of particles, which is more amenable to be cre-

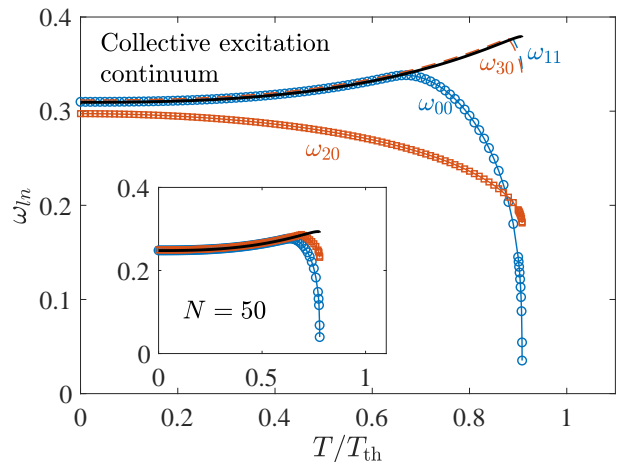


FIG. 8. Excitation frequencies  $\omega_{ln}$  ( $l \leq 9$  and  $n \leq 2$ ) of a small self-bound Bose droplet ( $N = 100$ ), as a function of the reduced temperature  $T/T_{\text{th}}$ . The red dashed curves show the surface modes  $\omega_{l \geq 2, n=0}$  and the blue dash-dotted curves show the compressional bulk modes. The lowest surface mode  $\omega_{20}$  (i.e., quadruple mode) and the lowest bulk mode (breathing mode) are highlighted by the red open squares and blue open circles, respectively. The black thick curve shows the threshold  $-\mu$ . At this number of particles, most of the excitation modes enter the collective excitation continuum with a frequency  $\omega_{ln} \geq -\mu$ . The inset shows the excitation spectrum at an even smaller number of particles,  $N = 50$ .

ated in the current experimental setups [6, 8]. In Fig. 7, we show the density distribution of a  $N = 100$  Bose droplet at two temperatures:  $T = 0$  (solid curve) and  $T = 0.7T_{\text{th}}$  (dashed curve). Compared with a large Bose droplet in Fig. 5, the density distribution of a small droplet shows a more appreciable temperature dependence. In particular, the center density can change up to several tens of percent (see the inset), as we increase the temperature towards the threshold. This pronounced temperature dependence could be related to the loss of the flat-top structure in the density distribution due to the reduced number of particles. A small Bose droplet appears to be more easier to be altered than a large droplet.

In Fig. 8, we report the temperature evolution of the collective excitation spectrum at  $N = 100$ . At this number of particles and at zero temperature, only the lowest surface mode (i.e., the quadruple mode  $\omega_{20}$ ) is bounded below the particle-emission threshold  $|\mu|$  [16]. When we increase temperature, the quadruple mode frequency decreases notably, presumably due to the increase of the droplet radius, since the droplet at this size acquires a more sensitive temperature dependence as we mentioned earlier. Interestingly, at about  $0.7T_{\text{th}}$  the frequency of the lowest compression bulk mode, the breathing mode frequency, starts to fall off the particle-emission threshold. It becomes increasingly softened towards the threshold temperature  $T_{\text{th}}$ . At an even higher temperature (i.e.,  $T \sim 0.87T_{\text{th}}$ ), more and more higher-order bulk modes

fall off the the particle-emission threshold and becomes softened. This fall-off feature turns out to be very general, occurring also at smaller number of particles, as can be seen in the inset for the selected case of  $N = 50$ .

The mode frequency softening, for both surface modes and compressional bulk modes in large and small Bose droplets, is therefore a characteristic feature of the thermally-induced droplet-to-gas transition at finite temperature. The mode softening effectively removes the excitation-forbidden interval in the number of particles predicted by Petrov at zero temperature [16], and opens the possibility to observe a small Bose droplet with non-zero temperature.

#### IV. CONCLUSIONS

In summary, we have theoretically investigated the finite-temperature effects on the structure and collective excitations of an ultradilute quantum droplet in free space, formed in a binary Bose-Bose mixture with inter-species attractions near the mean-field collapse. Our calculations are based on the extended (time-dependent) Gross-Pitaevskii equation generalized to the finite-temperature case. The density distribution is determined by solving the static Gross-Pitaevskii equation, while the collective excitation spectrum is obtained by solving the coupled Bogoliubov equations.

We have found a rich finite-temperature phase diagram as a function of the number of particles in the droplet. In particular, the critical number of particles at the droplet-to-gas transition is found to depend sensitively on the temperature. The excitation-forbidden interval predicted by Petrov is shown to shrink with increasing temperature and disappear completely at about  $0.73T_{\text{th}}$ , where  $T_{\text{th}}$  is the threshold temperature for thermally destabilizing an infinitely large Bose droplet. Above the temperature  $0.73T_{\text{th}}$ , there is at least one discrete collective mode below the particle-emission threshold, which may block the self-evaporation of the Bose droplet and allow a small but nonzero temperature.

Our results could be experimentally examined, if we are able to overcome the difficulty of finding a useful thermometry to measure the temperature. Qualitatively, at the number of particles slightly below  $N_{\text{th}}(T = 0) \simeq 94.2$ , the experimental observation of discrete quadrupole mode frequency or breathing mode frequency below the particle-emission threshold, i.e.,  $\omega_{20} < |\mu|$  or  $\omega_{00} < |\mu|$ , would be a very strong evidence for the finite-temperature effect.

#### ACKNOWLEDGMENTS

This research was supported by the Australian Research Council's (ARC) Discovery Program, Grants No. DE180100592 and No. DP190100815 (J.W.), Grant No. DP180102018 (X.-J.L), and Grant No. DP170104008 (H.H.).

#### Appendix A: Numerical method

Here, we describe our numerical approach to find the ground state solution of the static extended GPE Eq. (16), which is equivalent to minimize an energy density functional  $\mathcal{E}/N$ , where  $N = \int d\mathbf{r}|\phi_0(\mathbf{r})|^2$ . The energy functional in the free-space is given by,

$$\mathcal{E} = \langle K \rangle + \langle \mathcal{F} \rangle, \quad (\text{A1})$$

where

$$\langle K \rangle = -\frac{1}{2} \int d\mathbf{r} \phi_0(\mathbf{r}) \nabla^2 \phi_0(\mathbf{r}), \quad (\text{A2})$$

and

$$\langle \mathcal{F} \rangle = \int d\mathbf{r} \mathcal{F}(\mathbf{r}). \quad (\text{A3})$$

Here  $\mathcal{F}(\mathbf{r})$  is given by Eq. (13), with  $\mathbf{r}$ -dependency explicitly written out.

Due to the spherical symmetry of the system, we only consider the  $s$ -wave solution ( $l = 0$ ). Therefore, Eq.(16) reduces to an effective 1D radial equation. We first expand the condensed wave function in a 5-th order  $B$ -splines basis [42]:

$$\phi_0(\mathbf{r}) = \frac{1}{\sqrt{4\pi}} \sum_n c_n \frac{b_n(r)}{r}. \quad (\text{A4})$$

$B$ -spline basis has been extensively used in solving Schrödinger equations in two- and three-body problems with high accuracy [43, 44].  $B$ -spline basis allows to use an uneven grid, which might better represent the solution wave-function.  $B$ -spline basis also allows a higher order approximation of the derivative operator that appears in the kinetic energy term. The energy density functional  $\mathcal{E}/N$  then can be regarded as a non-linear function of coefficients  $c_n$ , which can be minimized using the standard conjugate-gradient method via software package such as "minFunc" in Matlab [45].

---

[1] For a recent review, see, for example, F. Böttcher, J.-N. Schmidt, J. Hertkorn, K. S. H. Ng, S. D. Graham, M. Guo, T. Langen, and T. Pfau, New states of matter with fine-tuned interactions: quantum droplets and dipolar supersolids, arXiv:2007.06391 (2020).

[2] I. Ferrier-Barbut, H. Kadau, M. Schmitt, M. Wenzel, and T. Pfau, Observation of Quantum Droplets in a Strongly Dipolar Bose Gas, Phys. Rev. Lett. **116**, 215301 (2016).

[3] M. Schmitt, M. Wenzel, F. Böttcher, I. Ferrier-Barbut, and T. Pfau, Self-bound droplets of a dilute magnetic

- quantum liquid, *Nature (London)* **539**, 259 (2016).
- [4] L. Chomaz, S. Baier, D. Petter, M. J. Mark, F. Wächtler, L. Santos, and F. Ferlaino, Quantum-Fluctuation-Driven Crossover from a Dilute Bose-Einstein Condensate to a Macrodroplet in a Dipolar Quantum Fluid, *Phys. Rev. X* **6**, 041039 (2016).
- [5] F. Böttcher, M. Wenzel, J.-N. Schmidt, M. Guo, T. Langen, I. Ferrier-Barbut, T. Pfau, R. Bombín, J. Sánchez-Baena, J. Boronat, and F. Mazzanti, Dilute dipolar quantum droplets beyond the extended Gross-Pitaevskii equation, *Phys. Rev. Research* **1**, 033088 (2019).
- [6] C. Cabrera, L. Tanzi, J. Sanz, B. Naylor, P. Thomas, P. Cheiney, and L. Tarruell, Quantum liquid droplets in a mixture of Bose-Einstein condensates, *Science* **359**, 301 (2018).
- [7] P. Cheiney, C. R. Cabrera, J. Sanz, B. Naylor, L. Tanzi, and L. Tarruell, Bright Soliton to Quantum Droplet Transition in a Mixture of Bose-Einstein Condensates, *Phys. Rev. Lett.* **120**, 135301 (2018).
- [8] G. Semeghini, G. Ferioli, L. Masi, C. Mazzinghi, L. Wolswijk, F. Minardi, M. Modugno, G. Modugno, M. Inguscio, and M. Fattori, Self-Bound Quantum Droplets of Atomic Mixtures in Free Space, *Phys. Rev. Lett.* **120**, 235301 (2018).
- [9] G. Ferioli, G. Semeghini, L. Masi, G. Giusti, G. Modugno, M. Inguscio, A. Gallelli, A. Recati, and M. Fattori, Collisions of Self-Bound Quantum Droplets, *Phys. Rev. Lett.* **122**, 090401 (2019).
- [10] C. D'Errico, A. Burchianti, M. Prevedelli, L. Salasnich, F. Ancilotto, M. Modugno, F. Minardi, and C. Fort, Observation of quantum droplets in a heteronuclear bosonic mixture, *Phys. Rev. Research* **1**, 033155 (2019).
- [11] D. Wang, Quantum Droplet in Heteronuclear Double Bose-Einstein Condensates, talk at IAS Workshop on Quantum Simulation of Novel Phenomena with Ultracold Atoms (May 6-7, 2019).
- [12] M. Barranco, R. Guardiola, S. Hernández, R. Mayol, J. Navarro, and M. Pi, Helium Nanodroplets: an Overview, *J. Low Temp. Phys.* **142**, 1 (2006).
- [13] O. Gessner and A. F. Vilesov, Imaging Quantum Vortices in Superfluid Helium Droplets, *Annu. Rev. Phys. Chem.* **70**, 173 (2019).
- [14] F. Dalfovo, S. Giorgini, L. P. Pitaevskii, and S. Stringari, Theory of Bose-Einstein condensation in trapped gases, *Rev. Mod. Phys.* **71**, 463 (1999).
- [15] C. Chin, R. Grimm, P. Julienne, and E. Tiesinga, Feshbach resonances in ultracold gases, *Rev. Mod. Phys.* **82**, 1225 (2010).
- [16] D. S. Petrov, Quantum Mechanical Stabilization of a Collapsing Bose-Bose Mixture, *Phys. Rev. Lett.* **115**, 155302 (2015).
- [17] D. S. Petrov and G. E. Astrakharchik, Ultradilute Low-Dimensional Liquids, *Phys. Rev. Lett.* **117**, 100401 (2016).
- [18] D. Baillie, R. M. Wilson, R. N. Bisset, and P. B. Blakie, Self-bound dipolar droplet: A localized matter wave in free space, *Phys. Rev. A* **94**, 021602(R) (2016).
- [19] F. Wächtler and L. Santos, Ground-state properties and elementary excitations of quantum droplets in dipolar Bose-Einstein condensates, *Phys. Rev. A* **94**, 043618 (2016).
- [20] Y. Li, Z. Luo, Y. Liu, Z. Chen, C. Huang, S. Fu, H. Tan, and B. A. Malomed, Two-dimensional solitons and quantum droplets supported by competing self- and cross-interactions in spin-orbit-coupled condensates, *New J. Phys.* **19**, 113043 (2017).
- [21] A. Cappellaro, T. Macrì, and L. Salasnich, Collective modes across the soliton-droplet crossover in binary Bose mixtures, *Phys. Rev. A* **97**, 053623 (2018).
- [22] G. E. Astrakharchik and B. A. Malomed, Dynamics of one-dimensional quantum droplets, *Phys. Rev. A* **98**, 013631 (2018).
- [23] X. Cui, Spin-orbit-coupling-induced quantum droplet in ultracold Bose-Fermi mixtures, *Phys. Rev. A* **98**, 023630 (2018).
- [24] C. Staudinger, F. Mazzanti and R. E. Zillich, Self-bound Bose mixtures, *Phys. Rev. A* **98**, 023633 (2018).
- [25] F. Ancilotto, M. Barranco, M. Guilleumas and M. Pi, *Phys. Rev. A* **98**, 053623 (2018).
- [26] L. Parisi G.E. Astrakharchik, and S. Giorgini, Liquid State of One-Dimensional Bose Mixtures: A Quantum Monte Carlo Study, *Phys. Rev. Lett.* **122**, 105302 (2019).
- [27] E. Aybar and M. Ö. Oktel, Temperature-dependent density profiles of dipolar droplets, *Phys. Rev. A* **99**, 013620 (2019).
- [28] V. Cikojević, L. Vranješ Markić, G. E. Astrakharchik, and J. Boronat, Universality in ultradilute liquid Bose-Bose mixtures, *Phys. Rev. A* **99**, 023618 (2019).
- [29] E. Chiquillo, Low-dimensional self-bound quantum Rabi-coupled bosonic droplets, *Phys. Rev. A* **99**, 051601(R) (2019).
- [30] F. Minardi, F. Ancilotto, A. Burchianti, C. D'Errico, C. Fort, and M. Modugno, Effective expression of the Lee-Huang-Yang energy functional for heteronuclear mixtures, *Phys. Rev. A* **100**, 063636 (2019).
- [31] M. Tylutki, G. E. Astrakharchik, B. A. Malomed, and D. S. Petrov, Collective excitations of a one-dimensional quantum droplet, *Phys. Rev. A* **101**, 051601(R) (2020).
- [32] H. Hu and X.-J. Liu, Consistent theory of self-bound quantum droplets with bosonic pairing, arXiv:2005.08581v1 (2020); to appear in *Physical Review Letters*.
- [33] H. Hu, J. Wang, and X.-J. Liu, Microscopic pairing theory of a binary Bose mixture with inter-species attractions: bosonic BEC-BCS crossover and ultradilute low-dimensional quantum droplets, *Phys. Rev. A* **102**, 043301 (2020).
- [34] H. Hu and X.-J. Liu, Microscopic derivation of the extended Gross-Pitaevskii equation for quantum droplets in binary Bose mixtures, *Phys. Rev. A* **102**, 043302 (2020).
- [35] Y. Wang, L. Guo, S. Yi, and T. Shi, Theory for Self-Bound States of Dipolar Bose-Einstein Condensates, *Phys. Rev. Research* **2**, 043074 (2020).
- [36] T. D. Lee, K. Huang, and C. N. Yang, Eigenvalues and Eigenfunctions of a Bose System of Hard Spheres and Its Low-Temperature Properties, *Phys. Rev.* **106**, 1135 (1957).
- [37] J. Wang, H. Hu, and X.-J. Liu, Thermal destabilization of self-bound ultradilute quantum droplets, *New J. Phys.* **22**, 103044 (2020).
- [38] M. Ota and G. E. Astrakharchik, Beyond Lee-Huang-Yang description of self-bound Bose mixtures, *SciPost Phys.* **9**, 020 (2020).
- [39] H. Pu and N. P. Bigelow, Properties of Two-Species Bose Condensates, *Phys. Rev. Lett.* **80**, 1130 (1998).
- [40] H. Hu and X.-J. Liu, Collective excitations of a spherical ultradilute quantum droplet, arXiv:2008.04629 (2020); to

appear in Physical Review A.

- [41] D. A. W. Hutchinson, E. Zaremba, and A. Griffin, Finite Temperature Excitations of a Trapped Bose Gas, Phys. Rev. Lett. **78**, 1842 (1997).
- [42] C. de Boor, *A Practical Guide to Splines* (Springer, New York, 1978).
- [43] H. W. van der Hart, *B-spline methods in R-matrix theory for scattering in two-electron systems*, J. Phys. B: At. Mol. Opt. Phys. **30**, 453 (1997).
- [44] J. Wang and C. H. Greene, Quantum-defect analysis of  $3p$  and  $3d$   $H_3$  Rydberg energy levels, Phys. Rev. A. **82**, 022506 (2010).
- [45] M. Schmidt, minFunc: unconstrained differentiable multivariate optimization in Matlab. <http://www.cs.ubc.ca/~schmidtm/Software/minFunc.html>, (2005).